DOE/SF/20720--71

FINAL REPORT

U.S. Department of Energy NLUF Grant # DE-FG03-95SF20720

TITLE: Temperature-Dependent Tensile Strength, Surface Roughness Diagnostics, and Magnetic Support and Positioning of Polymer ICF Shells

Principal Investigator: Arnold Honig, Phys. Dept, Syracuse University, Syr., NY 13244
Co-Investigator at L.L.E: Roger Q. Gram
Contributors to the work at Syracuse: M. Dong, Q. Fan, C.-K. Hsu, N. Miles, X. Wei

Period: April 17, 1995 - July 31, 1996.
Report preparation date: August 15, 1997

ABSTRACT

The research carried out under this grant is a continuation of some of our previous experimental work on ICF target shells which focused on emissivity properties over a large temperature range, and on magnetic properties which could lead to successful levitation of target shells. Former methods in which contact-less shell temperature determination was achieved by accurate measurements of shell permeation rate are not workable at temperatures below about 230K, since the permeation rate becomes too slow. A new method explored here for emissivity determination at lower temperatures than in the preceding studies utilizes visual observation of phase changes between the liquid and gaseous phases as the shell warms up under the influence of black-body radiation absorption. The apparatus for this method was modified from its previously form by using cold flowing gas as coolant rather than a liquid N_2 bath. Two gases, argon and methane, were principally employed. While the actual emissivities were not accurately measured here, proof of the method was established. CH_4 (methane) gives the best results, thus extending the temperature range of emissivity determination down to about 140K. For emissivity determinations at still lower temperatures, another method discussed in our previous work provides contact-less temperature measurement via the Curie law through measurements of the magnetic susceptibility using electron spin resonance (ESR). Current work showed some interesting distinctions among variously doped shells, but otherwise the results of the preliminary work carried out at the end of the previous grant were confirmed.

DISCLAIMER

I. INTRODUCTION

Since the interruption several years ago of our work on ICF spin-polarized D fuel due to the upgrading of OMEGA, we have concentrated our efforts on characterization of polystyrene target shells and developed novel techniques for determining the emissivity of the shells at low temperature, important for limiting the cryogenic target shell warming rate just prior to a shot. These have been described in a previous final report[1], and in a recent publication[2]. In this report, we describe progress made in these efforts during the grant period, in particular extension of the temperature range of the emissivity determinations by using a new method.

NLUF has supported our work over the previous decade, and it helps put into context our current work by briefly discussing in this introduction the principal mission of our original enterprise, use of spin-polarized fuel for fusion. It is relevant since it may be worthwhile to consider its revival with the new upgraded OMEGA. Our investigations began with a multifaceted program aimed at preparing and imploding polystyrene targets containing solid spin-polarized HD or D_2 fuel. This program was brought to an advanced stage, including cold (4K) transfer of solid deuterium-filled target shells prepared at Syracuse and transported, positioned and shot at the OMEGA facility at the University of Rochester's Laboratory for Laser Energetics (LLE). Due to the shutdown of OMEGA for its upgrade, the final experiments using spin-polarized solid HD targets were not completed. Nevertheless, the entire deuterium polarization technology has now been fully developed and demonstrated[3] and the impetus for spin-polarized fusion has not diminished. It is most probable that the polarized fuel technology we developed will be utilized again within the next few years. In addition, the 4K cold-transfer[4] technology we introduced formed the basis of the current cryotarget development for OMEGA upgrade.
In the course of the earlier work, we developed a strong capability for characterizing polymer target shells by techniques not readily accessible at other centers, and since the closing of (old) OMEGA, we have focused our attention on target shell properties such as emissivity and accommodation coefficient, which are of high concern to the cryogenic ICF program, both for polarized and unpolarized fuels. In direct drive ICF experiments, the emissivity determines the warm-up rate under room temperature black-body

irradiation during the short interval between retracting the shroud, in order to make the target accessible to the laser beams, and the firing of the lasers. Since there are mechanical constraints which limit the speed with which the shroud can be retracted and since the black body radiation environment is difficult to alter, emissivity controls the target shell temperature rise. For polarized targets, an appreciable temperature rise leads to relaxation-induced depolarization, and must be avoided. For an unpolarized target, the temperature rise must also be held to a very low value to avoid distortion of the required highly-symmetrized condensed fuel layer. For a given residual gas pressure in the fusion chamber, a low accommodation coefficient[5] reduces the temperature rise rate due to free molecular conduction. Even with indirect drive, shell warming from black-body radiation can be a significant detrimental factor.

Both emissivity and accommodation coefficient are less than or equal to 1, and lower values of these, which result in slower warming of the target, are always advantageous to ICF for the reasons presented above. During the grant period preceding this one, we had improved upon the techniques first introduced at the Monterey Ninth Target Specialists' meeting[6] in 1993, and at the Albuquerque Tenth Target Specialists' meeting[7], for investigation of emissivity and accommodation coefficients of target shells. The improvements were principally with respect to target conductive thermal isolation and optical access. The measurements of both emissivity and accommodation coefficient are reliable and in the vicinity of 10^{-2}, a very satisfactory range for temperature stability of polystyrene-based cryogenic ICF targets. In our previous final report[1], we also included initial experiments on magnetic properties of shells, obtained by doping styrene with magnetic particles of a few nm diameter prior to forming the shells by a microencapsulation or drop tower method, and results of experiments on paramagnetic shells obtained by stabilization at low temperatures of paramagnetic defects produced by gas discharge plasma (GDP) coatings. The idea of using room temperature stable organic radical dopants[8] in styrene to make paramagnetic polystyrene shells was introduced. The paramagnetism with which the shells become endowed would permit contactless temperature sensing via electron spin resonance (ESR) measurements, owing to the Curie law. Such measurements are applicable all the way down to the liquid helium temperature

region, enabling extension of our target shell emissivity and accommodation coefficient measurements to the temperature region where they will be actually employed. Other suggested applications of such paramagnetic shells to ICF include levitation of target shells at low temperatures for non-perturbative shell positioning and possibly shell transport, and uniform or possibly even profiled shell heating in the liquid hydrogen temperature range through electron spin resonance and relaxation.

During this grant period, further work on these aspects was carried out, but the main effort was on emissivity determination in the intermediate temperature region between about 100K and 240K. A new technique of contactless temperature measurement in this range was introduced for this, consisting of visual observation of phase changes of selected gases.

II. EMISSIVITY AND ACCOMMODATION COEFFICIENT MEASUREMENTS ON POLYSTYRENE ICF TARGET SHELLS

Emissivity and accommodation coefficient measurements are of importance for both direct and indirect drive inertial confinement fusion, as mentioned in the preceding section. Our previous measurements in the >240K range are, to our knowledge, the first for polystyrene polymer shells. The results of that work have been presented at conferences[6,7] and in a publication[2]. A brief description of the method is reviewed here, since some of the technical implementation is common to the new visual observation method as well.

The experiments are thermal transfer ones in which a shell of known heat capacity is subject to warming by absorbing radiation from a known isothermal environment, in our case the walls of the cell containing the target shell. These walls, at temperature T_W, are maintained warmer than the shell temperature, T_S. The shell is mounted on thin spider silks, and hence is thermally isolated with respect to heat conduction from its support structure. Thus, heat transfer to the shell is via net radiation absorption and via gas conduction. The radiative heat transfer rate is proportional to $e_S(T_W^4 - T_S^4)$, where e_S is the shell emisivity. The gas pressure is arranged to be always low, so that the heat transfer rate via gas conduction is characteristic of the molecular free conduction (as opposed to

diffusion) regime. Its contribution to the heat transfer rate is proportional to $a_S P_C (T_W - T_S)$, where a_S is the accommodation coefficient[5] of the shell and P_C is the gas pressure in the cell. Because of the different temperature dependencies of the heat-transfer-rate, and the ability to control the pressure range, separation of each of these thermal transport contributions to the temperature rise of the shell can be effected by monitoring the target shell temperature during warm-up. The innovative element of these experiments is in the means of monitoring the shell temperature, T_S. The shells are very small and any external thermometer placed in contact with them would compromise the conductive isolation and make the interpretation of the measurements difficult, or indeed even impossible. We introduced a method whereby the property of a shell called its permeability coefficient, which is proportional to the rate at which gas leaks out of the shell into a vacuum, serves as the thermometric indicator. This quantity, denoted by K_P, depends exponentially on the temperature of the shell. One measures the gas leakage *rate* out of the shell by continuously monitoring the pressure in its containment cell. This method works very well in the temperature region of 240 - 350K. Below 240K, the permeation rate is too slow. Nevertheless, these 'high' temperature values are helpful for approximating the low temperature values, and other contactless temperature determination methods for shells which can be utilized at lower temperatures have been proposed by us. Among these are the magnetic susceptibility one, which has been mentioned above, and visual observation of phase transitions at boiling and melting points of various materials, which has been carried out by us during the past year and is the principal subject of this report.

In both the permeation rate and visual phase transition techniques, a polystyrene target shell is mounted on very low thermal conductance spider silks and placed in a small sample cell whose walls are maintained at any desired temperature, T_W, between 77K and 350K. In the permeation method, visual access is not necessary whereas in the phase transition method, it clearly is. The shell temperature, T_S, can be cooled to a low value, for example 77K, at which any gas inside it cannot leak out since the shell is very impermeable at low temperature. The sample chamber is connected via a thin tube to a larger volume which includes an accurate pressure sensor in the low pressure regime, in our case a Baratron operable over the pressure range 0 to 2000 Pa. The experimental

arrangement, including provision for permeating gas into the shell, cooling the sample cell with flowing gas, and optical access is shown in Fig. 1. This is the configuration used in the principal work reported here. A detail of one form of sample cell utilized by us, where the shell is glued to a pair of spider silk supports, is seen in Fig. 2. This particular stalk mounted arrangement is useful when only permeation is measured, since the optical path is obviously blocked by the stalk. An alternative arrangement in which the shell is glued to supporting spider silks with optical access is shown in Fig. 3. Another shell positioning method we have successfully employed places the shell freely on a net of spider silks, such as is shown in Fig. 4. In this way, the shells are usable after being characterized. In both positioning methods, the targets are accessible for visual viewing through an Indium o-ring sealed window at the bottom of the cell, in a manner depicted best in Fig. 3. The aim is to cool the gas-filled target shell, quickly raise the temperature, T_W, of the sample cell walls, and observe the rise in T_S due to heat transport from the cell walls to the shell. Using the known values of polystyrene heat capacity[9], $C_V(T)$, and measurement of shell temperature as a function of time during the warm-up, the total rate of heat absorption of the shell, dQ_S/dt, is obtained from the product $C_V(T)(dT_S/dt)$. The procedure for the permeation rate measurements has been described in previous reports, so we turn our discussion at this point to the new method of visual observation of phase transitions for contactless temperature determination.

III. METHOD OF VISUAL OBSERVATION OF PHASE TRANSITIONS FOR EMISSIVITY DETERMINATION

This method has much in common with the previous one, regarding general concept, basic apparatus and procedures. The difference is in the contactless temperature measurement technique. Instead of using helium or deuterium gas at room temperature (293K) permeated into the target shell to about 12 atmospheres pressure, in this method we use gases which have phase transitions in the required temperature regions.

For the temperature range between 77K and 240K, several gases are available, among them Ar, O_2, CH_4, Xe. We experimented with Ar and CH_4, but for demonstration of the method, CH_4 was chosen since its thermodynamic characteristics[10] are better

matched to the current apparatus. However, the other gases should present no special difficulties. The concept is the same as for the previous permeation based temperature measurement method. A target is mounted in a conductively isolated manner with spider silks or equivalent material. The apparatus including the illumination system has been presented in Fig. 1. An important change for the experiment to be described is the wall temperature surrounding the target is cooled by cold gas, and not by immersion in a cold liquid. This prevents bubbling interference in the image, and refractive effects from the cooling liquid. The cooling gas is helium which passes through a tube situated in liquid nitrogen. By varying the rate of gas flow, the temperature can be controlled. With our set-up, it is difficult to attain temperatures below about 100K, but this is more than adequate for the methane experiments, and usable for the Argon as well.

We measured the polystyrene permeation rate at room temperature for Argon and for Methane. Fig. 5a shows the room temperature leak-out from a polystyrene shell initially filled to 12 atmospheres with Argon, and Fig. 5b gives the background-leak-corrected results. From the latter, the leak-out, or permeation time constant, τ, is determined. From the relation between τ, the dimensional physical characteristics of the shell (given in the caption), and the permeation constant K_p,

$$\tau = \frac{wr}{3K_pRT_S}, \qquad (1)$$

we determine the permeation constant to be 5.9 X 10^{-16} mole/Pa.m.s, about an order of magnitude smaller than the permeability constant for helium or deuterium in polystyrene[1]. Figure 6 similarly shows the results of a badkground-corrected permeation time constant determination for methane, from which the permeation constant, K_p, is determined to be 2.3 X 10^{-15} mole/Pa.m.s. It is apparent that the permeation constant for Argon is lower than for methane, and partly for that reason, and also because of the more favorable phase transition temperatures for methane with respect to this initial apparatus, methane was the gas of choice for demonstrating the method.

This demonstration experiment was not intended to provide an accurate value of the emissivity, but to demonstrate that this visual method is a workable one. The delicate 5 μm spider silks usually used to support the shell were replaced with thicker fibers, roughly 40 μm in diameter. This makes the target more stable against the vibration

problems in this not very elaborate new apparatus, but increases the thermally conductive effects enough to limit the accuracy of an emissivity measurement. This can be seen by estimating the relative heat input contributions from radiative and conductive mechanisms, using an arbitrary 10K temperature difference, in the 140K range. The dQ/dt's are 1.4 μW for the radiative contribution, using an emissivity of 0.2, and 1.5 μW for the conductive contribution, using a thermal conductivity value of 1.3 μW/cm.K, approximately that of teflon™ at 140K. By constructing a more stable apparatus and returning to spider silk supports, the radiative heat input would exceed the conductive one and the emissivities would be more easily determinable. Meanwhile, we limit our objective to demonstrating the utility of the contactless thermometry aspect. From the above heat transfer rates and the heat capacities and latent heat of vaporization of CH_4, the vaporization phase transition is expected to take a few minutes, under the conditions of our experiment, and the shell warming rate should be about 30K/min. Since the experiment is done while the T of the surrounding cryostat rises at a rate of about 1K/min, the temperatures of the shell should be within a few degrees of that of the cryostat, rather than the 10K difference assumed in the calculation. The temperature difference could increase to about 10K during the liquid vaporization process.

The target was permeated with methane to a pressure of 50 atmospheres, in slow increments so that it could withstand possible implosion during the intervals of non-equilibrium between shell internal pressure and cell external pressure. This high a pressure was judged necessary, since for the shell used, of diameter 575 μm and wall thickness 9.5 μm, if a uniformly condensed layer formed upon condensation, it would be about 5 μm thick, easily discerned optically from the changed index of refraction and from scattering. The results of Fig. 6 were used to obtain the safe filling intervals. When equilibrium at 50 atmospheres is achieved, the gas supply source is shut off, and the cell and target shell are cooled. Since they cool at nearly the same rate, only small pressure differentials exist between the cell and the target shell. In the old procedure of Ref. 1, when the temperature became colder, the permeation rate slowed sufficiently to evacuate the cell. Here, even allowing for pressure reduction from the gas law, there was the possibility of the shell exploding under the approximately 30 atmosphere pressure

differential. Thus, for the first test, both cell and target were cooled together, and warmed together, with exchange gas present in the cell. Optical effects are expected from both the condensed liquid in the target and the condensed liquid in the cell, which we shall see. A later experiment was done in which the cell was pumped after cooling. It turned out that the shell withstood the evolving pressure differentials as the system warmed, consistent with the upper part of the range of polystyrene tensile strengths, near 80 MPa. Such an experiment with proper low thermal conductivity supports should be capable of yielding good emissivity values.

Considerable difficulty in maintaining a good image was encountered when liquid N_2 filled the dewar. The bubbling and convective instabilities effectively precluded keeping a constant image, using the apparatus we assembled for these preliminary experiments. In principle, both the illumination system and dewar mount could be designed to minimize these perturbations, and the method could be used down to 77K. In our case, we opted for circulating the cold helium gas as described before, through the dewar, as shown in Fig. 1. In this way, we could not cool below 100K, but this was sufficient for demonstrating the method for CH_4.

IV. RESULTS OF VISUALIZED PHASE TRANSITION EXPERIMENTS

As discussed above, two types of experiments were undertaken. In the first, we cooled the cryostat to 100K, and then cut off the circulating cool helium gas and allowed the system to warm, in the presence of exchange gas in the cell. Figure 7 depicts the cooling and warming temperature profile of the container cell upon which the thermocouple is mounted, with numbers marking positions at which "still" photographs were taken. We expect this temperature profile is quite similar to that of the target shell itself, because of the presence of exchange gas and the fairly high conductance of the supporting fibers. Figs. 8 and 9 show a series of photos of the shell taken with the long distance microscope camera and displayed on the monitor, which correspond to a few selected numbered points on the temperature profile curves (Fig. 7). We have interpreted these pictures in the following way:

No optical changes are observed as the gas cools inside the cell and inside the target, as seen in the photographs corresponding to temperature points 1 and 2, shown on Fig. 8.

Formation of a liquid pool at the bottom of the cell having lens-like qualities causes an apparent shrinkage of the image at the temperature corresponding to point 5 on Fig. 8.

A slightly lagging formation of liquid inside the target shell is seen at temperature point 6 in Fig. 8.

Vaporization of the liquid, inside and outside the cell, as the cell and target warm through temperature points (referring to Fig. 7) up to 12, are shown in Fig. 9.

After this experiment, which demonstrates the visibility of features associated with the phase changes, the second experiment, in which pump-out is effected at the temperature corresponding to point 6 on Fig. 8, was undertaken. After the pump-out, and during the warm-up, a feature associated only with vaporization inside the target, and lagging in temperature rise because of the absence of exchange gas, was observed. As mentioned previously, one cannot calculate accurately the emissivity because of the high thermal conductance of the target supports in this present experiment, which makes it difficult to extract just the radiative contribution. However, the existence of the visual feature inside the target shell shows that the method is an operable one. Video recordings of the cooling and warming processes in both experiments were made, but "still" pictures were not taken in the second experiments in which the exchange gas was pumped at the lowest temperature point. Its cool-down portion is the same as shown in Fig. 8, but the warm-up presents fewer features because of the absence of liquid or gas in the cell itself.

V. ADDITIONAL SUSCEPTIBILITY MEASUREMENTS

Several shells were examined using the ESR method described in our previous final report[1] for this project. The results were basically similar to those previously reported. However, a new observed feature is that the spin-density measured for GDP shells of germanium doped polystyrene can exceed that for the plain polystyrene shells

by up to an order of magnitude. These observations are perhaps worth further investigation.

REFERENCES

1. Final Report, Grant No. DE-FG03-93SF20144, Dec 15, 1995. A. Honig, P. I.
2. A. Honig, Q. Fan, C.-K. Hsu and X. Wei, Fusion Technology 28, 1859 (1995).
3. A. Honig., Q. Fan, X. Wei, M. Breuer, J. P. Didelez, M. Rigney, M. Lowry, A. Sandorfi, A. Lewis, and S. Whisnant, 12th Intl. Symp. on High Energy Spin Physics, Amsterdam, Sept 1996. "Spin 96" Conference Proceedings, World Scientific, p. 365.
4. N. Alexander, J. Barden, Q. Fan, and A. Honig, Rev. Sci. Instrum. 62, 2729 (1991).
5. The accommodation coefficient is a measure of heat transport efficiency in the free molecular conduction pressure range, where the mean free path is of the order of the apparatus dimensions.
6. A. Honig, X. Wei, Q. Fan, N. Alexander and N. Palmer, 9th Target Fabrication Specialists' Meeting, Monterey, CA, July 6 - 8, 1993. LLNL Conf. Report: CONF9307127, L-14854-2.
7. A. Honig, Q. Fan, C.-K. Hsu and X. Wei, 10th Target Fabrication Specialists' Meeting,

   Feb. 6 - 10, 1995, Taos, NM. Los Alamos National Laboratories Publication Number LA-UR-95-29386.
8. A stable radical we have suggested using has the abbreviated name TEMPO. It is used for dynamically polarized nuclear targets.
9. The heat capacity $C_V(T)$ of polystyrene as a function of temperature is found in the Polymer Handbook, 3rd Ed. (1989). J. Brandup and E. H. Immergut, Eds. p. VI/389. At T = 300K, it is 1.27 J/g.K, At T = 140K, it is 0.61 J/g.K
10. For thermophysical data on methane, see for example Gas Encyclopaedia, published by L'Air Liquide, Division Scientifique; Elsevier Press (1976).

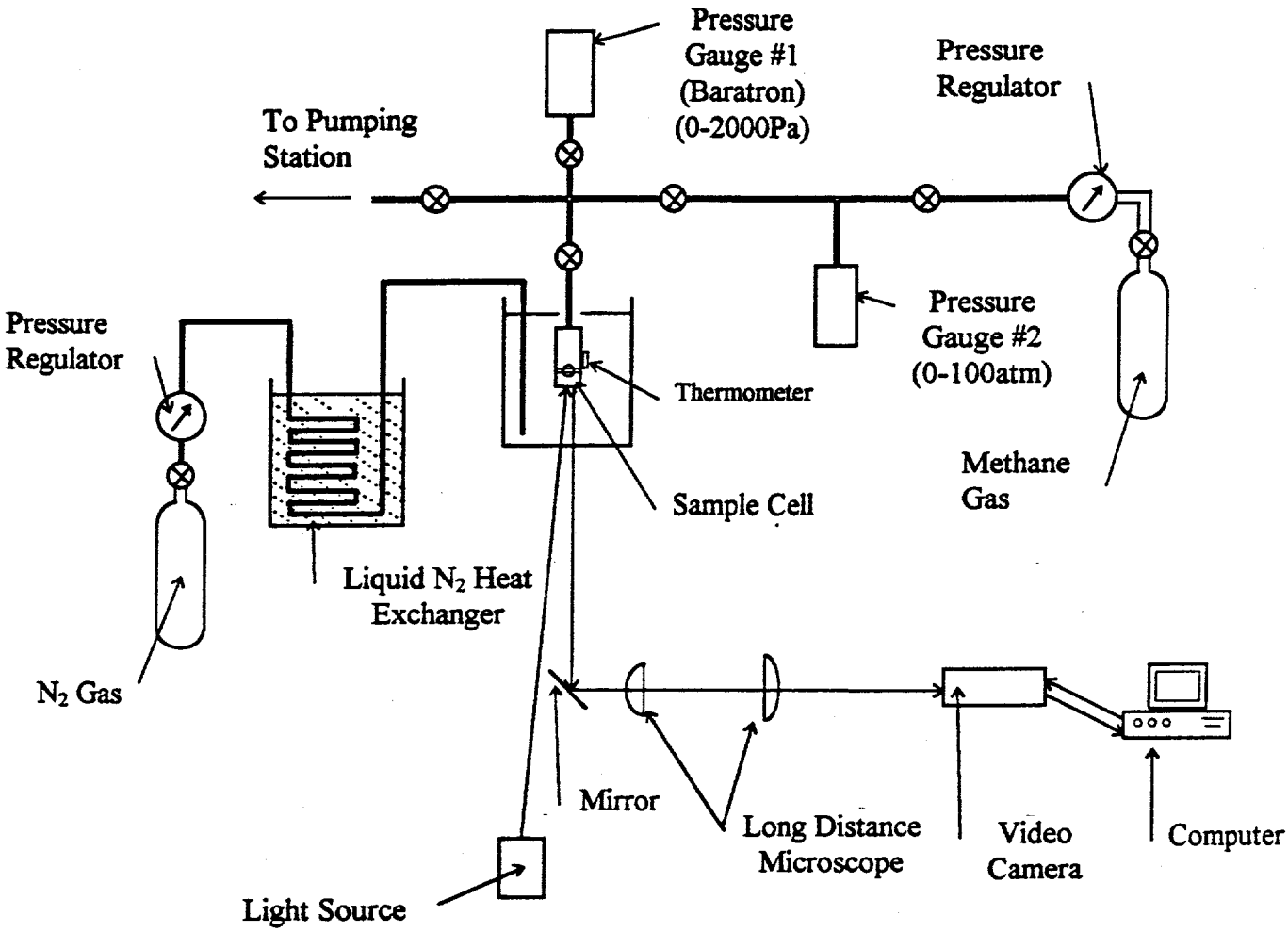

Fig. 1. Shell Permeation Apparatus with Optical Access and Temperature Control Using Cold Flowing Helium Gas

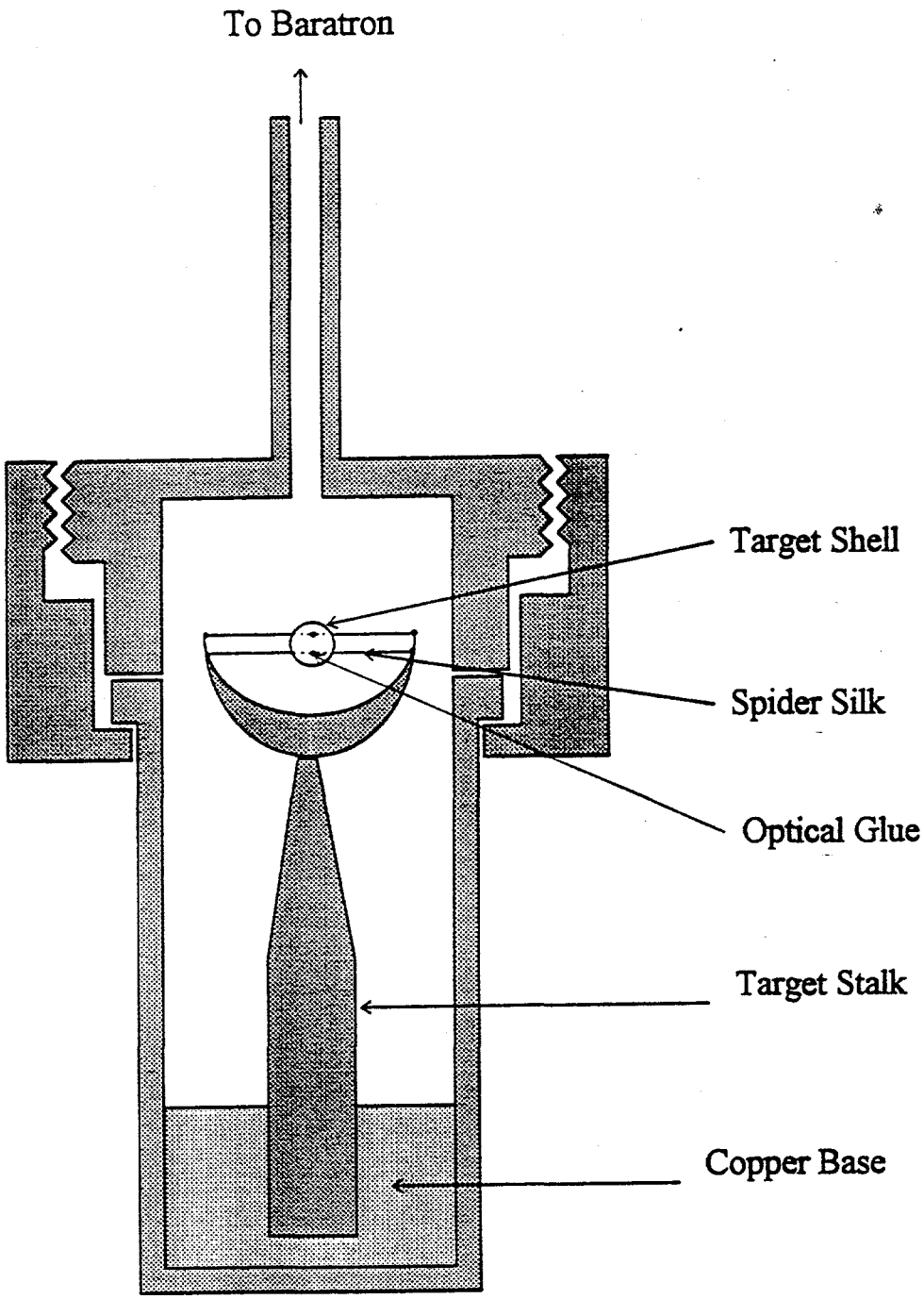

Fig. 2. Shell Mounted on a Stalk with Two Spider Silks. No Optical Access for the Shell.

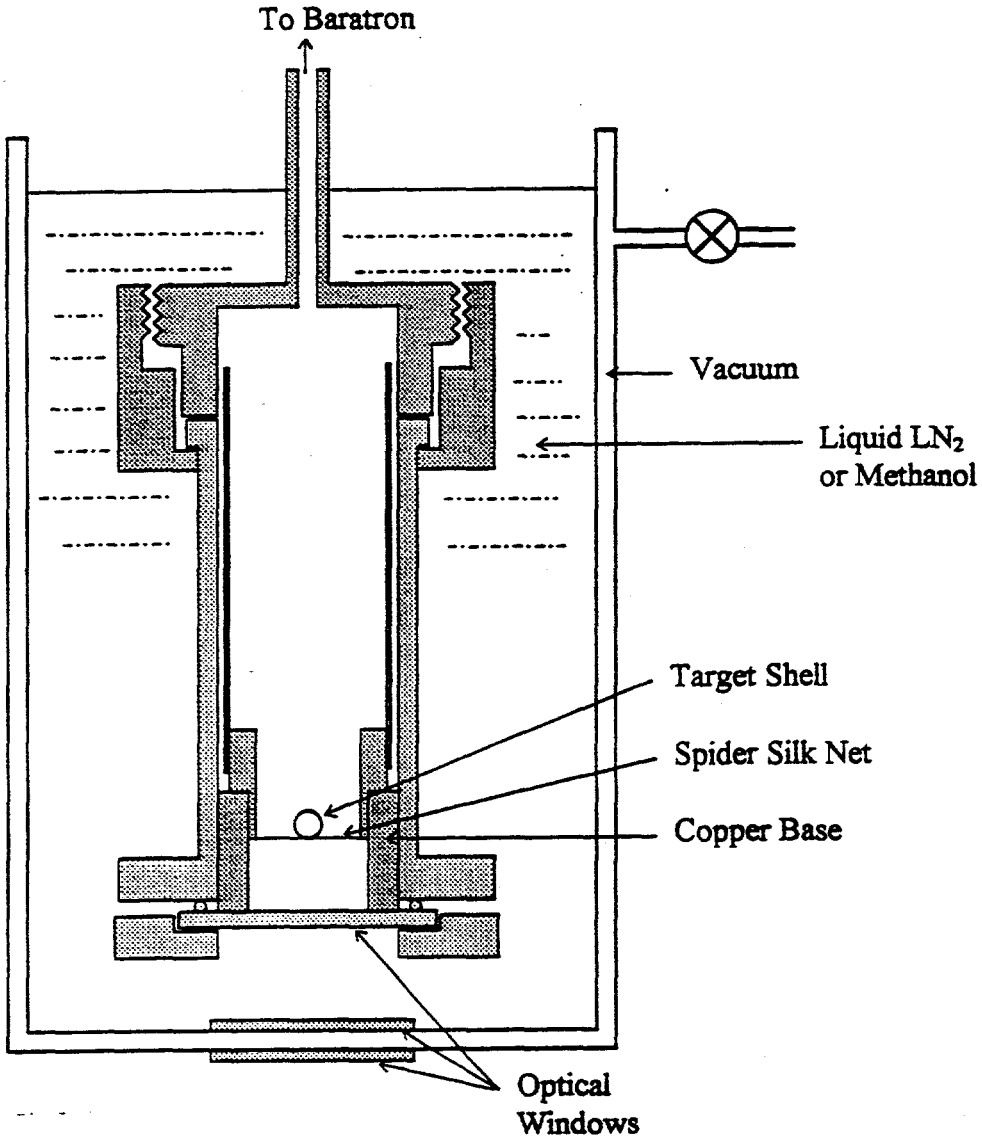

Fig. 3. Shell Mounted in the Cell Using Spider Silks Allowing Optical Access. Cell Window is Shown.

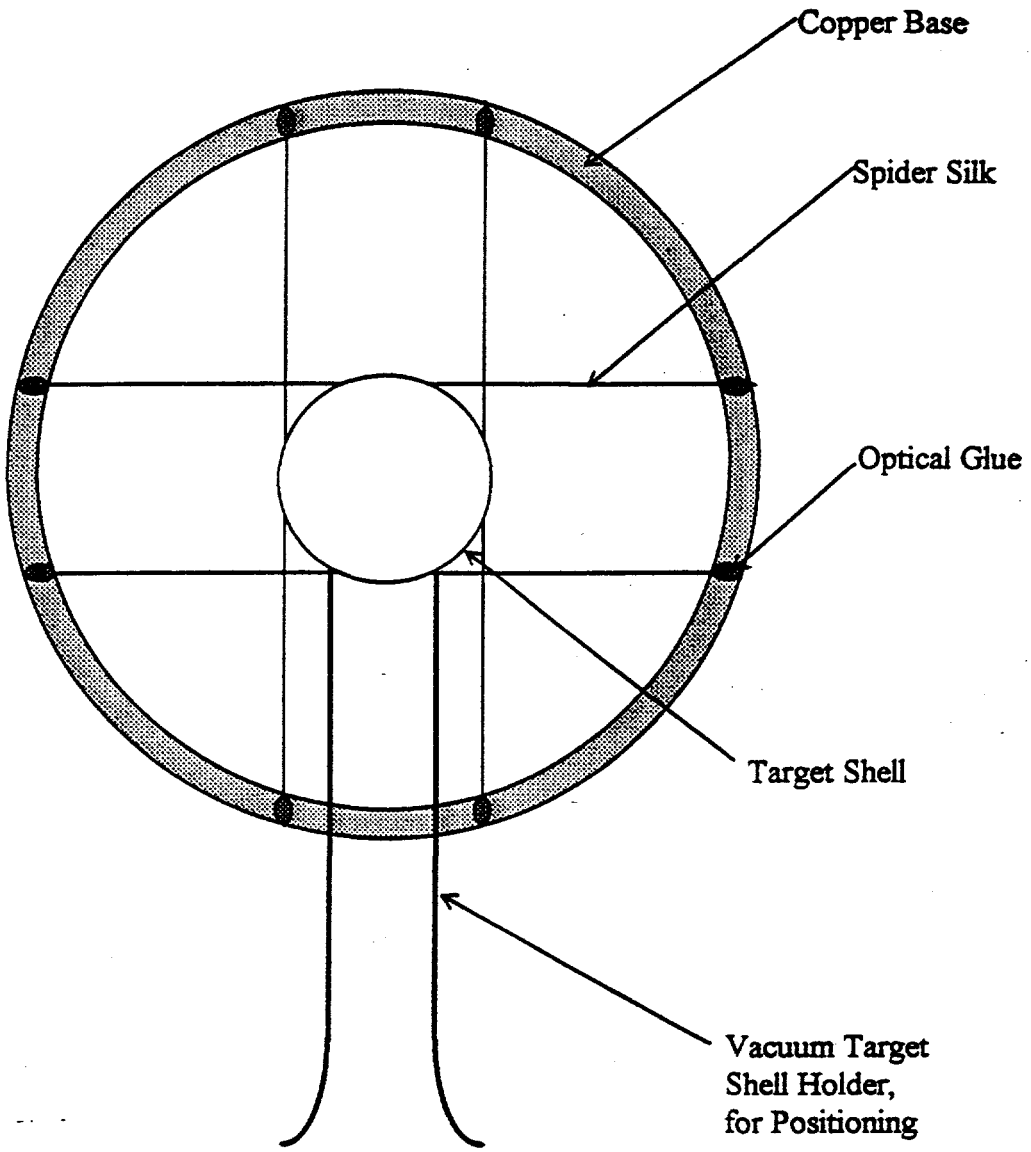

Fig. 4. Shell Freely Resting on a Spider Silk Net inside Cell with Optical Access

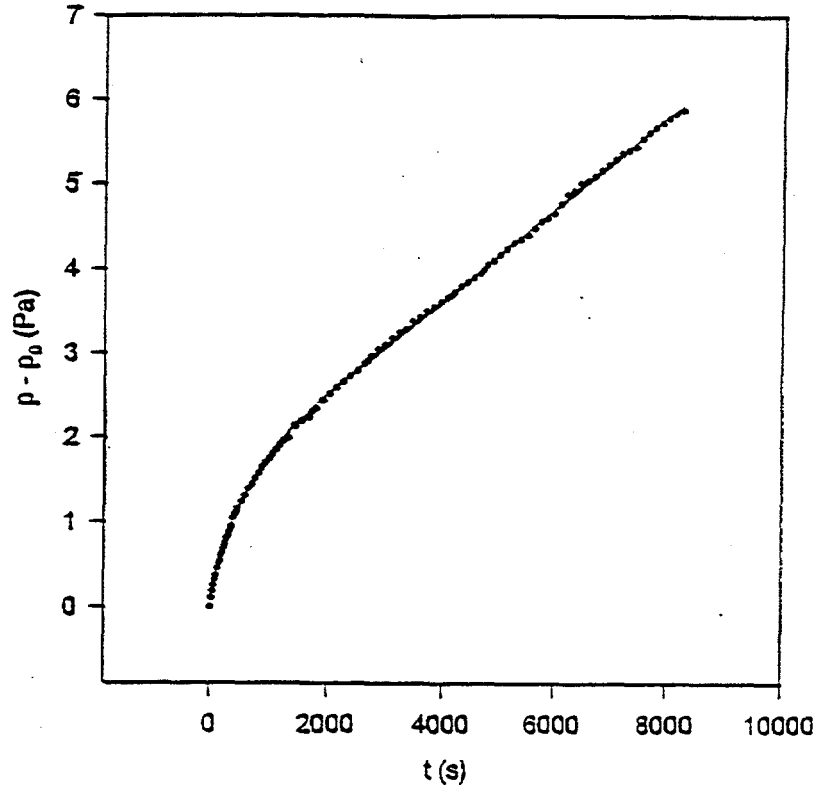

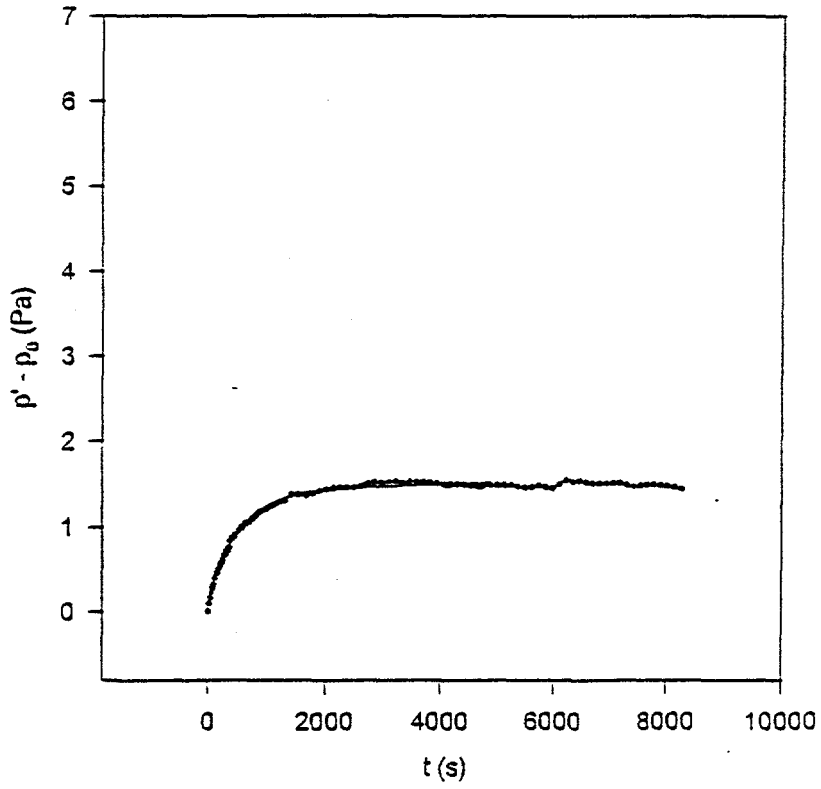

Fig. 5. Determination of Permeation Constant of Polystyrene for Argon Gas at T = 293K. Shell Parameters are: Diameter (O.D.) = 686 μm; Wall = 6.5 μm.

a) Without Background Correction.
b) With Background Correction

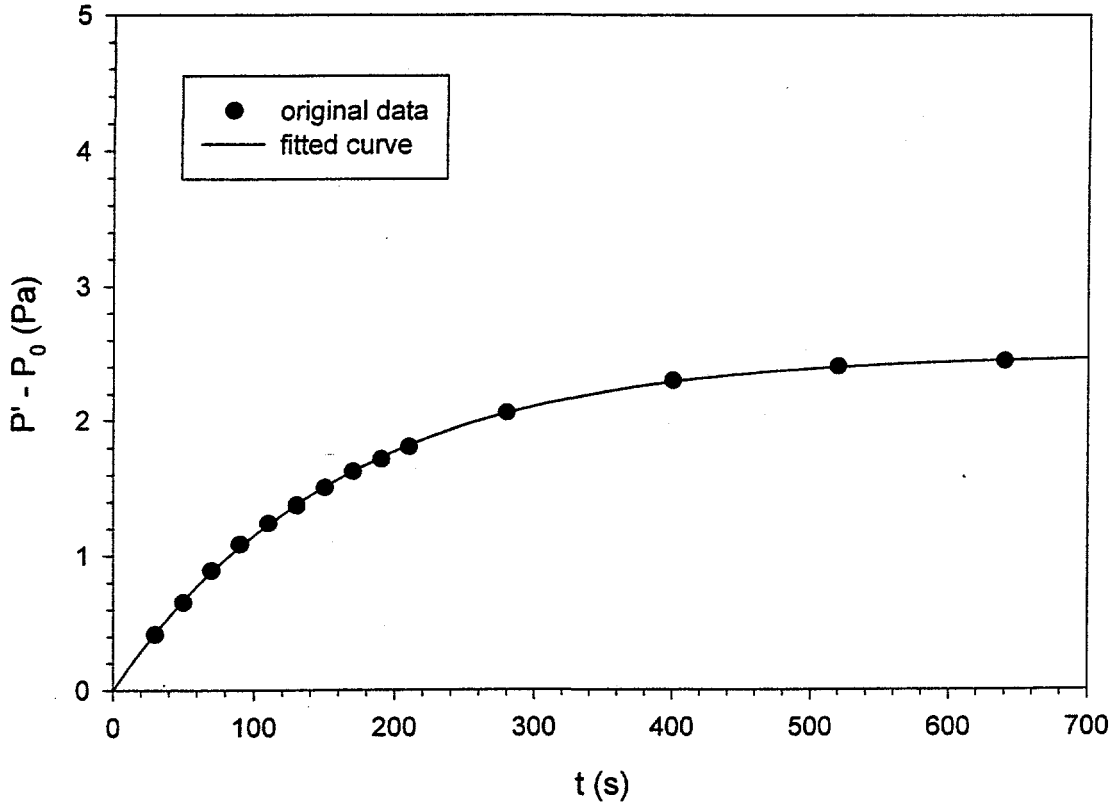

Fig. 6. Determination of Permeation Constant of Polystyrene for Methane Gas at T = 293K. Shell Parameters are: Diameter (O.D.) = 576 μm; Wall = 9.5 μm Correction Has Been Made for Background

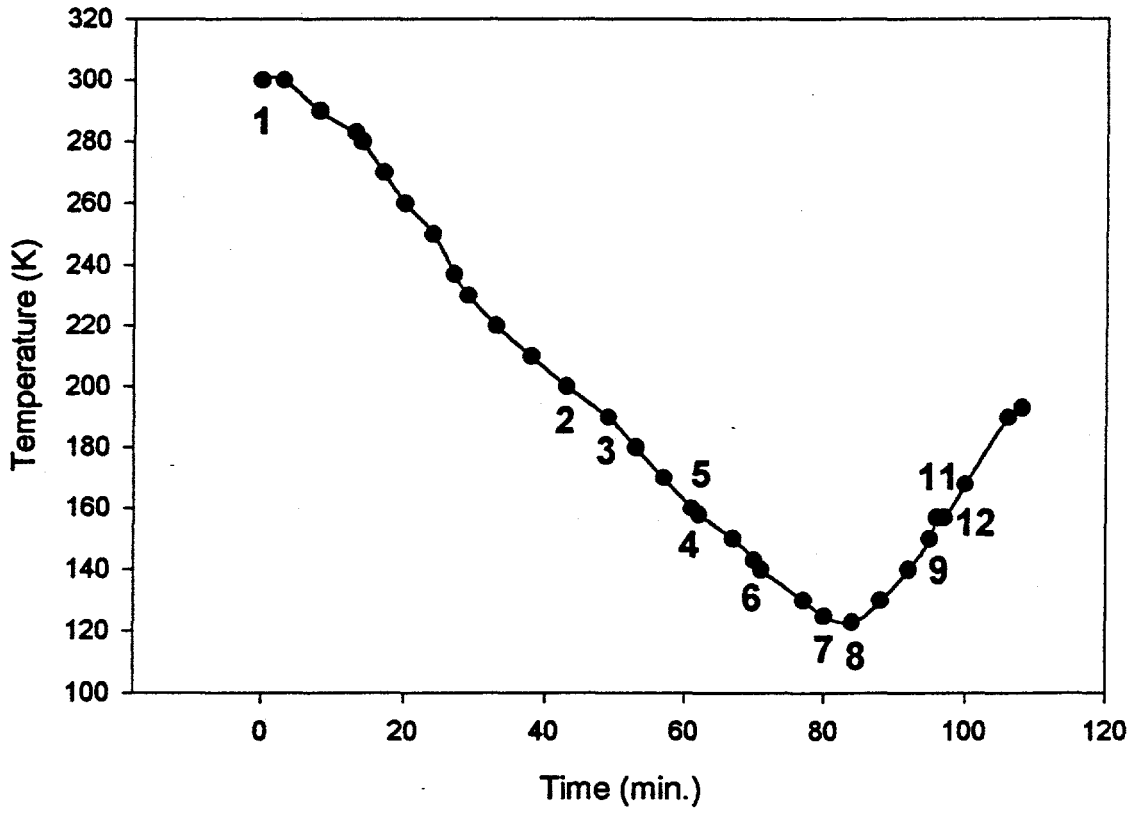

Fig. 7. Time Profile of Temperature of Flowing-Gas Cooled Cryostat During Shell Cooling and Warming Periods

Temperature Point 1

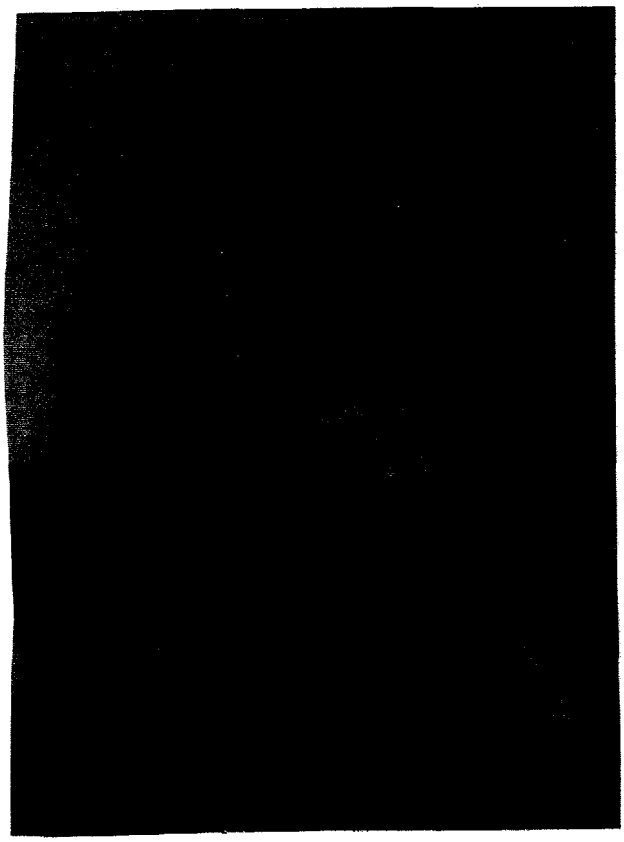

Temperature Point 2

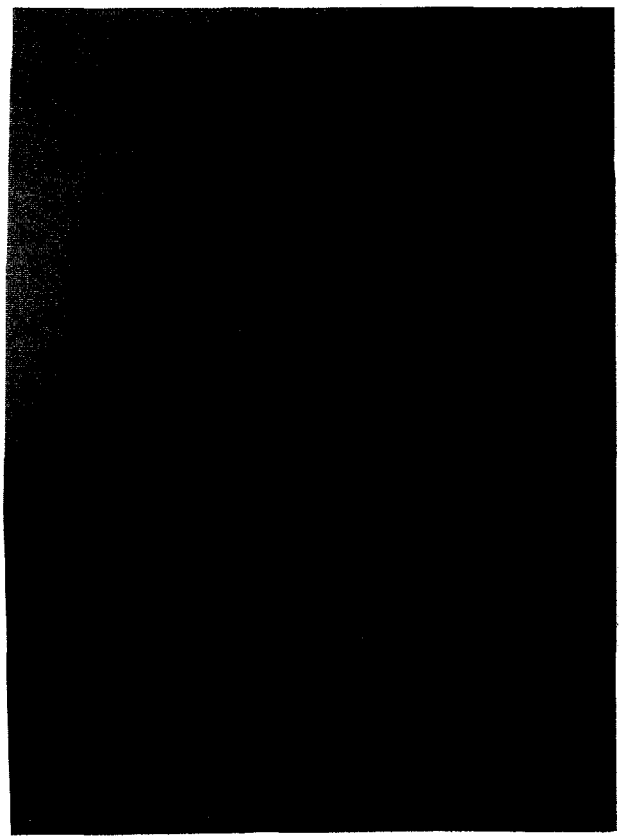

Temperature Point 5

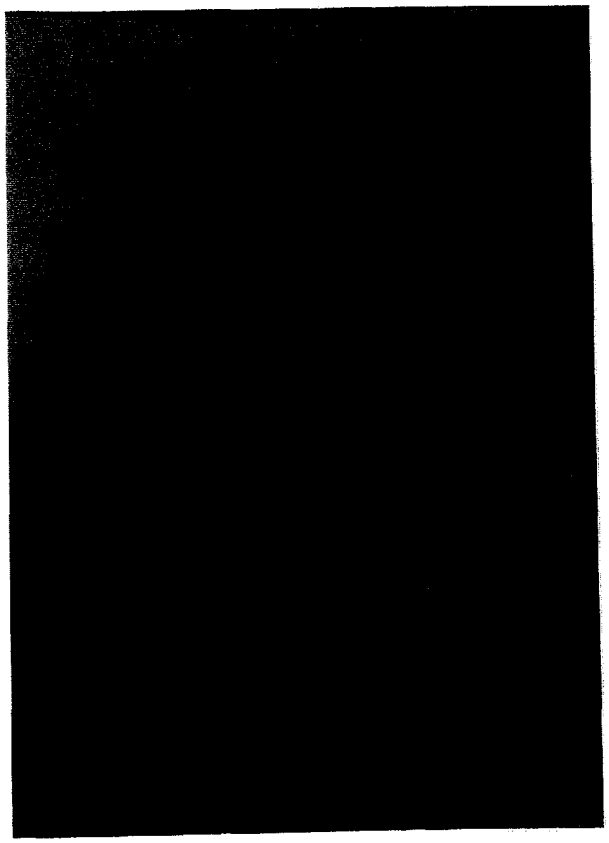

Temperature Point 6

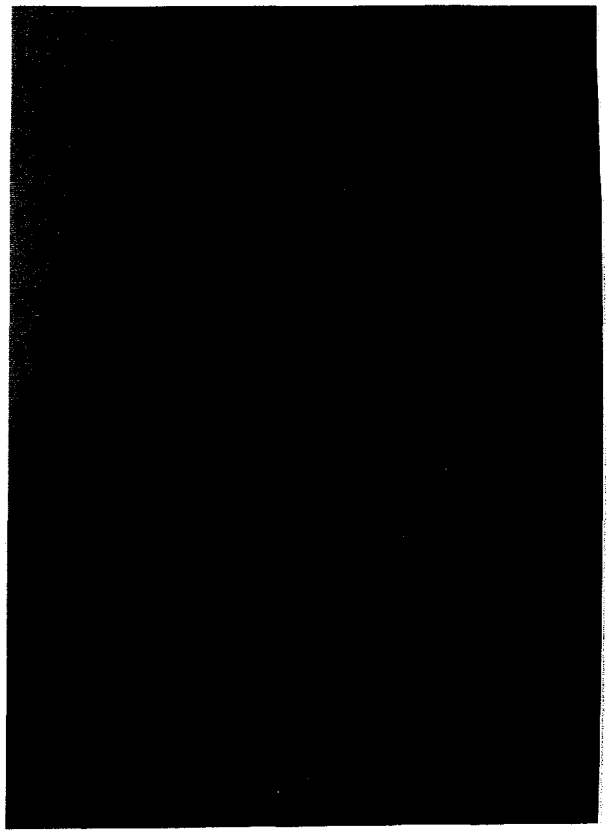

Fig. 8. Photos of Shell Taken from CCD Image Using Long-Distance Microscope, at Temperatures Corresponding to Numbered Points 1, 2, 5 and 6, on Fig. 7.

Temperature Point 8

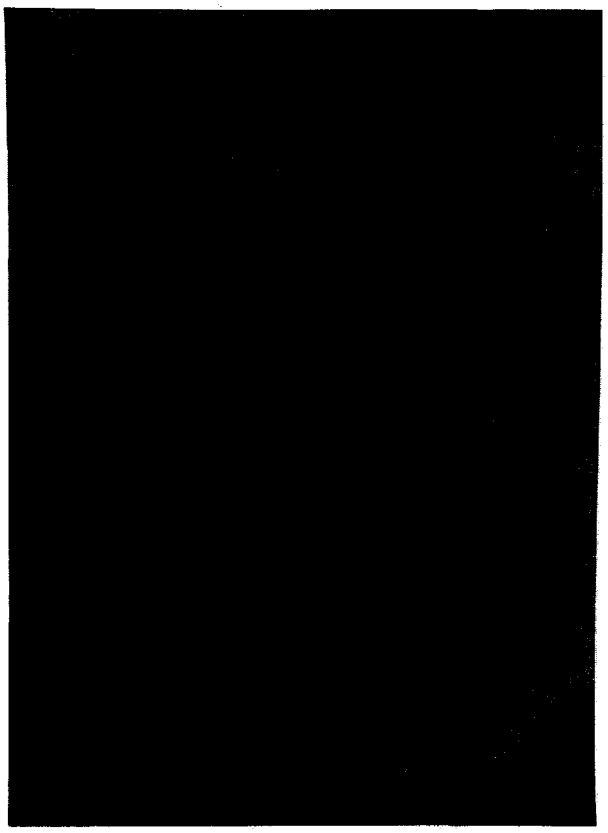

Temperature Point 9

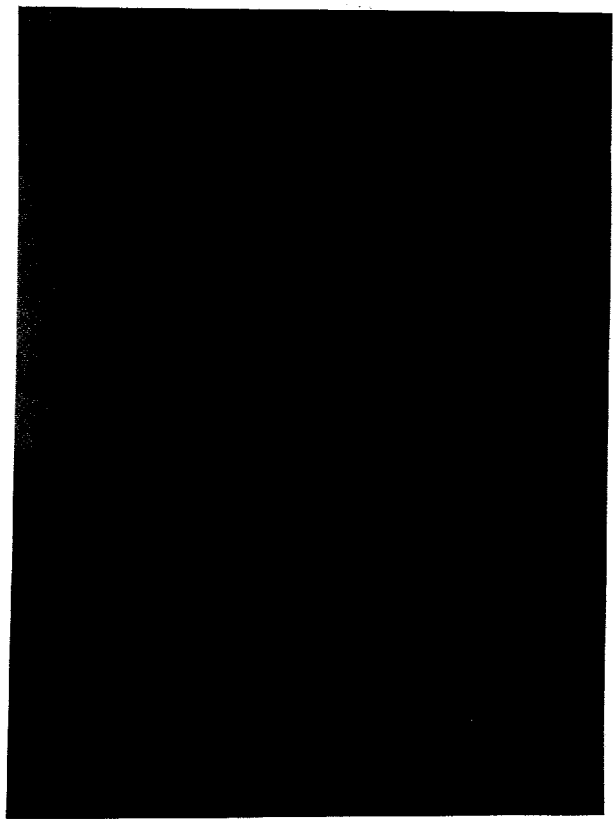

Temperature Point 11

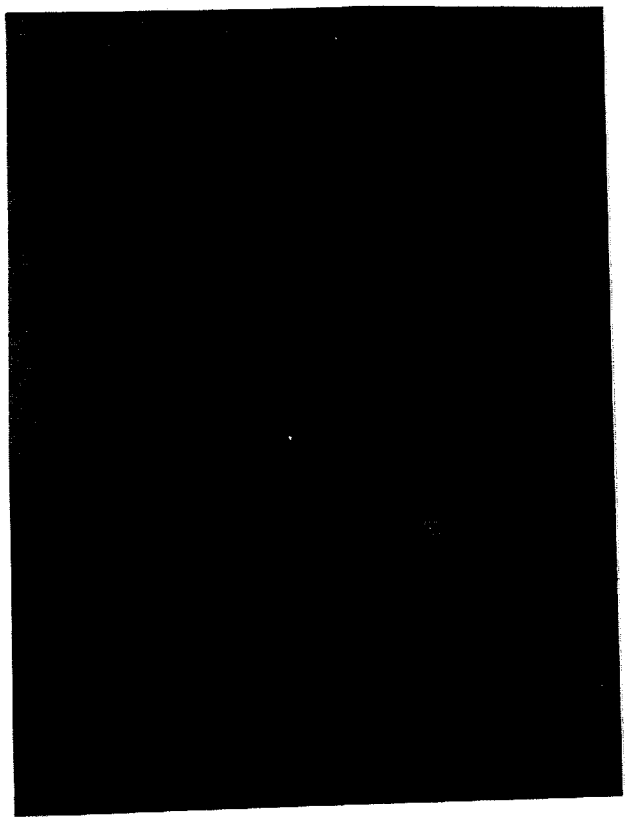

Temperature Point 12

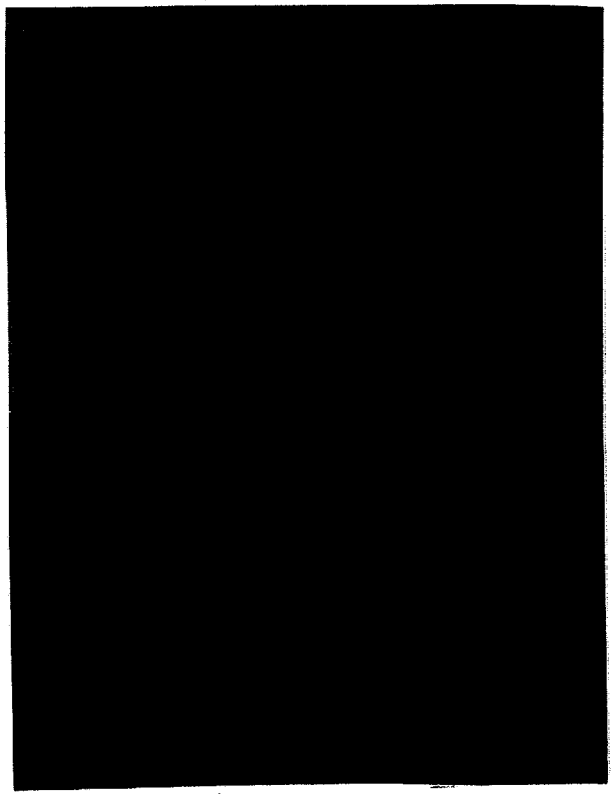

Fig. 9. Photos of Shell Taken from CCD Image Using Long-Distance Microscope, at Temperatures Corresponding to Numbered Points 8, 9, 11 and 12, on Fig. 7.